J Therm Anal Calorim (2015) 122:747–754
DOI 10.1007/s10973-015-4776-9

Thermodynamic properties and X-ray diffraction of $Bi_4Ti_3O_{12}$

A. V. Knyazev[1] · O. V. Krasheninnikova[1] · N. N. Smirnova[1] · A. N. Shushunov[1] · E. V. Syrov[1] · A. G. Blokhina[1]

Received: 21 February 2015 / Accepted: 9 May 2015 / Published online: 2 June 2015

Abstract The temperature dependence of heat capacity of $Bi_4Ti_3O_{12}$ has been measured for the first time in the range from 7 to 346 K by precision adiabatic vacuum calorimetry. The experimental data were used to calculate standard thermodynamic functions, namely the heat capacity, enthalpy $H^o(T) - H^o(0)$, entropy $S^o(T) - S^o(0)$, and Gibbs function $G^o(T) - H^o(0)$, in the range from $T \to 0$ to 346 K. The structure of $Bi_4Ti_3O_{12}$ is refined by the Rietveld method (space group $Fmmm$, $Z = 4$) at temperatures of 173, 273, 373, 473 K. Thermal deformation model is proposed on the basis of structural data.

Keywords Perovskite · Aurivillius phase · Adiabatic vacuum calorimetry · Heat capacity · Thermodynamic functions, thermal deformation model

Introduction

In recent years, bismuth-containing layered ferroelectrics, first described by Aurivillius [1–3], have been the subject of researchers' ever-increasing attention. The general formula of such compounds can be represented as $A_{m-1}Bi_2B_mO_{3m+3}$, where m is typically from 1 to 5 [4]. The A atoms most frequently have a valence of I, II, or III (or a combination of these) and a coordination number $CN_A > 6$. The B site is usually occupied by transition metals in octahedral coordination ($CN_B = 6$). The structure of these stoichiometric compounds is made up of slabs and blocks. Each slab consists of n layers of anion octahedra. For $n \to \infty$, its structure approaches the cubic perovskite structure. The blocks can be thought of as structural units of cubic BiF_3 [3]. Characteristically, the bismuth-containing layered ferroelectrics have low dielectric permittivity, high Curie temperatures, low temperature coefficients of their resonance frequency, highly anisotropic electromechanical coupling coefficients, and low aging rates [5–7].

The goals of this work include calorimetric determination of the temperature dependence of the heat capacity $C_p^o = f(T)$ of $Bi_4Ti_3O_{12}$ from 7 to 346 K, detection of the possible phase transitions, and calculation of the standard thermodynamic functions $C_p^o(T)$, $H^o(T) - H^o(0)$, $S^o(T) - S^o(0)$, and $G^o(T) - H^o(0)$ in the range from $T \to 0$ to 346 K. We also present results of X-ray diffraction studies depending on the temperature in order to obtain information on thermal deformation of this material.

Experimental

Sample

Tetrabismuth trititanium oxide was prepared by the solid-state reaction between titanium oxide and bismuth(III) nitrate pentahydrate (reaction 1). The synthesis was performed in a porcelain crucible, into which the reaction mixture with the atomic ratio 4Bi: 3Ti was loaded. The mixture was calcined at 1173 K for 50 h, undergoing regrinding every 10 h.

Electronic supplementary material The online version of this article (doi:10.1007/s10973-015-4776-9) contains supplementary material, which is available to authorized users.

✉ A. V. Knyazev
knyazevav@gmail.com

[1] N. I. Lobachevsky State university of Nizhni Novgorod, Gagarin Prospekt 23/2, 603950 Nizhny Novgorod, Russia

$$4Bi(NO_3)_3{\cdot}5H_2O + 3TiO_2 \rightarrow Bi_4Ti_3O_{12} + 12NO_2 + 3O_2 + 20H_2O \quad (1)$$

Apparatus and measurement procedure

For structural investigations, an X-ray diffraction pattern of a $Bi_4Ti_3O_{12}$ sample was recorded on a Shimadzu X-ray diffractometer XRD-6000 (Cu K_α radiation, geometry θ–2θ) in the 2θ range from 10° to 120° with scan increment of 0.02°. Rietveld analysis and structure refinement [8] were carried out using RIETAN-97 software [9]. The X-ray data and estimated impurity content (0.5–1 mass%) in the substance led us to conclude that the tetrabismuth trititanium oxide sample studied was an individual crystalline compound. The X-ray diffraction studies depending on the temperature were carried out on a Shimadzu X-ray diffractometer XRD-6000 using Attachment TTK-450 (Anton Paar).

Thermal analysis was carried out with a Setaram LABSYS DSC 1600 differential scanning calorimeter in an argon atmosphere at a heating rate of 0.0833 K s^{-1}.

To measure the heat capacity C_p^o of the tested substance in the range from 6 to 337 K, a BKT-3.0 automatic precision adiabatic vacuum calorimeter with discrete heating was used. The calorimeter design and the operation procedure were described earlier [10]. The calorimeter was tested by measuring the heat capacity of high-purity copper and reference samples of synthetic corundum and K-2 benzoic acid. The analysis of the results showed that measurement error of the heat capacity of the substance at helium temperatures was within ±2 %, then it decreased to ±0.5 % as the temperature was rising to 40 K, and was equal to ±0.2 % at $T > 40$ K. Temperatures of phase transitions can be determined with the error of ±0.02 K.

Results and discussion

Crystal structure

The structure of $Bi_4Ti_3O_{12}$ was refined assuming space group *F*mmm. The initial model included the atomic coordinates in the structure of tetrabismuth trititanium oxide, which was solved by Aurivillius [11]. The details of the X-ray diffraction experiments and structure refinement data are listed in Table 1. Figure 1 represents the measured, simulated, and difference X-ray diffraction patterns for $Bi_4Ti_3O_{12}$ ($T = 173$ K), as well as a pattern of lines corresponding to reflection maxima. There is a good agreement between the measured and simulated patterns. Table 2 lists the coordinates of the atoms and their isotropic thermal parameters.

The crystal structure of Aurivillius-phase layered perovskite $Bi_4Ti_3O_{12}$ is shown in Fig. 2a. $Bi_4Ti_3O_{12}$ has a general formula of $[Bi_2O_2]^{2+}[B_{m-1}M_mO_{3m+1}]^{2-}$, where B is the 12-fold-coordinated cation with low valence in the perovskite sublattice, M denotes the octahedral site occupied by the ions with high valence, and *m* is the number of perovskite layers between the $[Bi_2O_2]^{2+}$ blocks. The perovskite slabs of $Bi_4Ti_3O_{12}$ are composed of TiO_6 octahedrons and 12-fold-coordinated Bi^{3+} (atoms Bi_1) and are three layers in the thickness as shown in Fig. 2a. The $[Bi_2O_2]^{2+}$ blocks are constructed of square pyramids (atoms Bi2 are located in the central vertices).

Table 3 lists interatomic distances in the crystal structure of $Bi_4Ti_3O_{12}$. The bond lengths Ti–O in octahedra vary

Table 1 Details of the X-ray diffraction experiment and the results of the structure refinement for $Bi_4Ti_3O_{12}$

Temperature/K	173	273	373	473
Space group	*F*mmm	*F*mmm	*F*mmm	*F*mmm
Z	4	4	4	4
2θ range/°	10–120	10–120	10–120	10–120
a/Å	5.40255 (11)	5.40256 (15)	5.41098 (10)	5.41620 (10)
b/Å	5.44174 (11)	5.44065 (15)	5.44785 (10)	5.45167 (10)
c/Å	32.7837 (7)	32.7929 (9)	32.8501 (7)	32.8820 (7)
V/Å^3	963.82 (3)	963.90 (5)	968.36 (3)	970.92 (3)
Number of reflections	556	550	544	546
Number of refined parameters				
Structural parameters	13	13	13	13
Others	20	20	20	20
R_{wp}; R_p/%	5.59; 4.01	5.19; 3.76	5.71; 4.17	5.85; 4.25

$R_{wp} = \{(\Sigma w_i[y_{iobs} - y_{icalc}]^2/(\Sigma w_i[y_{iobs}]^2)\}^{1/2}$; $R_p = (\Sigma|y_{iobs} - y_{icalc}|)/(\Sigma y_{iobs})$

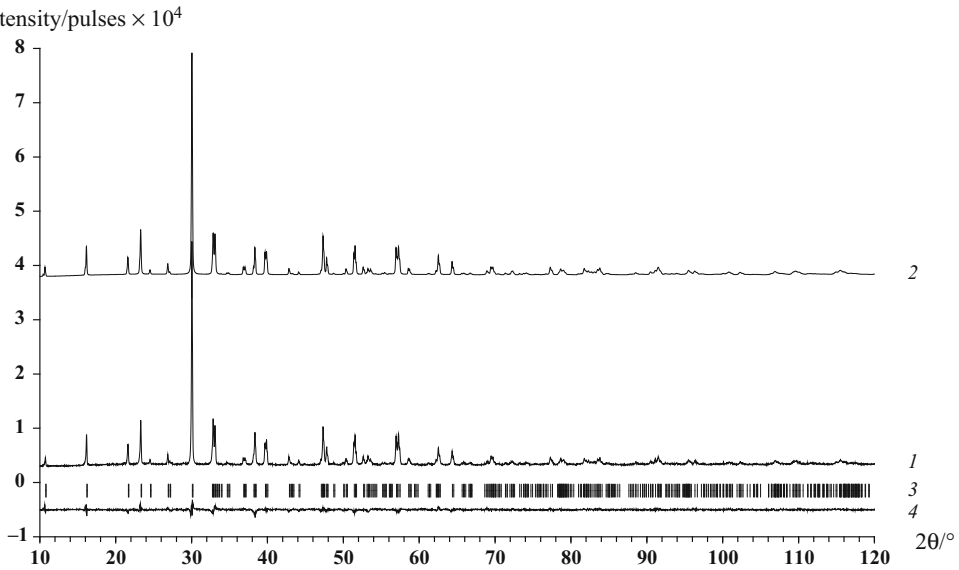

Fig. 1 Observed (*1*), simulated (*2*), and *four* difference X-ray diffraction patterns and *three* Bragg reflections for $Bi_4Ti_3O_{12}$

Table 2 Coordinates and isotropic thermal parameters of atoms in the structure of $Bi_4Ti_3O_{12}$

Atom	Site	*x*	*y*	*T* = 173 K		*T* = 273 K		*T* = 373 K		*T* = 473 K	
				z	B/Å^2	*z*	B/Å^2	*z*	B/Å^2	*z*	B/Å^2
Bi_1	8i	0	0	0.06698 (5)	0.05 (3)	0.06703 (5)	0.05 (3)	0.06707 (5)	0.31 (3)	0.06706 (5)	0.56 (3)
Bi2	8i	0	0	0.21106 (5)	0.05 (3)	0.21083 (5)	0.05 (3)	0.21100 (5)	0.31 (3)	0.21098 (5)	0.56 (3)
Ti1	4b	0	0	0.5	1.6 (3)	0.5	2.0 (4)	0.5	1.7 (3)	0.5	2.0 (3)
Ti2	8i	0	0	0.3697 (3)	3.5 (2)	0.3701 (3)	2.2 (2)	0.3708 (2)	2.2 (2)	0.3703 (2)	2.2 (2)
O_1	8e	0.25	0.25	0	3.3 (3)	0	3.0 (3)	0	3.5 (2)	0	3.6 (2)
O_2	8f	0.25	0.25	0.25	3.3 (3)	0.25	3.0 (3)	0.25	3.5 (2)	0.25	3.6 (2)
O_3	8i	0	0	0.4297 (9)	3.3 (3)	0.4347 (8)	3.0 (3)	0.4348 (7)	3.5 (2)	0.4312 (8)	3.6 (2)
O_4	8i	0	0	0.3154 (8)	3.3 (3)	0.3192 (8)	3.0 (3)	0.3197 (7)	3.5 (2)	0.3150 (8)	3.6 (2)
O_5	16j	0.25	0.25	0.1230 (5)	3.3 (3)	0.1222 (5)	3.0 (3)	0.1192 (5)	3.5 (2)	0.1190 (5)	3.6 (2)

in the range from 1.66 to 2.27 Å. It should be noted that the octahedra with a central atoms Ti2 are the most distorted.

Heat capacity

The C_p^o measurements were taken between 7 and 346 K. The mass of the sample loaded in the calorimetric ampoules of the BKT-3.0 device was 1.2657 g. Hundred and sixty-eight experimental C_p^o values were obtained in three series of experiments (Table 1S). The heat capacity of the sample varied from 20 to 50 % of the total heat capacity of calorimetric ampoule + substance over the range between 7 and 346 K. The experimental points of C_p^o in the temperature intervals between $T =$ (10 and 30) and (21 and 346) K were fitted by means of Eqs. (2, 3) of the C_p^o versus temperature have been obtained. The corresponding coefficients (A, B, C, etc.) are given in Table 4

$$C_p^o = A_1 + B_1 \cdot \left(\frac{T}{30}\right) + C_1 \cdot \left(\frac{T}{30}\right)^2 + D_1 \cdot \left(\frac{T}{30}\right)^3 + E_1 \cdot \left(\frac{T}{30}\right)^4 + F_1 \cdot \left(\frac{T}{30}\right)^5 + G_1 \cdot \left(\frac{T}{30}\right)^6 + H1 \cdot \left(\frac{T}{30}\right)^7 + I_1 \cdot \left(\frac{T}{30}\right)^8 + J_1 \cdot \left(\frac{T}{30}\right)^9 + K_1 \cdot \left(\frac{T}{30}\right)^{10} \quad (2)$$

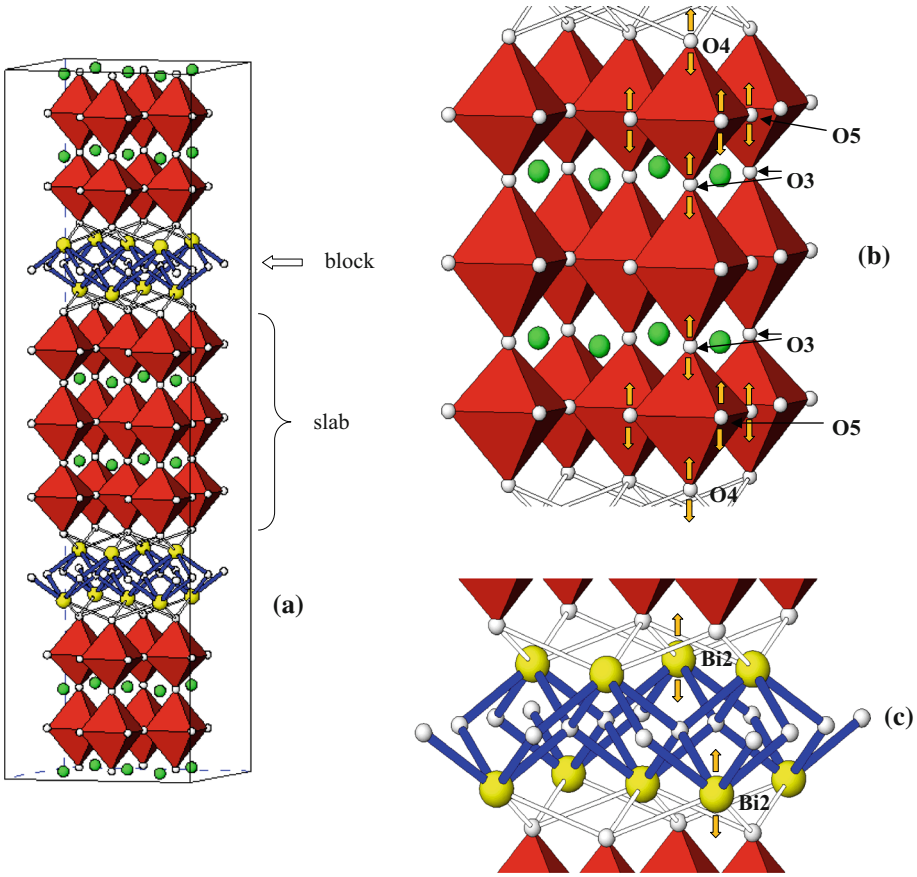

Fig. 2 The crystal structure (**a**) and fragments of the structure of $Bi_4Ti_3O_{12}$ (**b**—slab, **c**—block, *orange arrows*—atomic displacements)

$$\ln C_p^o = A_2 + B_2 \cdot \ln\left(\frac{T}{30}\right) + C_2 \cdot \ln^2\left(\frac{T}{30}\right) + D_2 \cdot \ln^3\left(\frac{T}{30}\right) + E_2 \cdot \ln^4\left(\frac{T}{30}\right) + F_2 \cdot \ln^5\left(\frac{T}{30}\right) + G_2 \cdot \ln^6\left(\frac{T}{30}\right) + H_2 \cdot \ln^7\left(\frac{T}{30}\right) + I_2 \cdot \ln^8\left(\frac{T}{30}\right) + J_2 \cdot \ln^9\left(\frac{T}{30}\right) + K_2 \cdot \ln^{10}\left(\frac{T}{30}\right) + L_2 \cdot \ln^{11}\left(\frac{T}{30}\right) + M_2 \cdot \ln^{12}\left(\frac{T}{30}\right) + N_2 \cdot \ln^{13}\left(\frac{T}{30}\right) \quad (3)$$

Their root mean square deviation from the averaging $C_p^o = f(T)$ curve was ±0.15 % in the range $T =$ (7 to 55) K, ±0.075 % from $T =$ (55–80) K and ±0.050 % between $T =$ (80 and 346) K.

The experimental values of the molar heat capacity of $Bi_4Ti_3O_{12}$ over the range from 7 to 346 K and the averaging $C_p^o = f(T)$ plot are shown in Figure 1S. The heat capacity C_p^o of this substance in interval from 7 to 346 K gradually increases with rising temperature and does not show any peculiarities.

From the experimental C_p^o values in the range 25–50 K, the value of the fractal dimension D of the tetrabismuth trititanium oxide was evaluated. According to the fractal theory of the heat capacity [12], D is the most important parameter that specifies the character of heterodynamics of the substance structure. For solids of a chain structure, the relation C_p^o versus T at lower temperatures is proportional to T^1, of a layer structure to T^2, and of steric one to T^3 [13]. In the fractal theory of the heat capacity, an exponent on T is the heat capacity function that is denoted by D and is called the fractal dimension. This follows specifically from Eq. (4) [12]:

$$C_v = 3D(D+1)kN\gamma(D+1)\xi(D+1)(T/\theta_{max})^D, \quad (4)$$

where N is the number of atoms in a formula unit, k is the Boltzmann constant, $\gamma(D+1)$ is the γ-function, $\xi(D+1)$ is the Riemann ξ-function, and θ_{max} is the characteristic temperature. As follows from inferences [12], D can be evaluated from the experimental data on the temperature-dependent heat capacities from a slope of the corresponding rectilinear sections of the plot ln C_v versus ln T. Without a substantial uncertainty, it may be assumed that at $T < 50$ K $C_p^o = C_v$. From the ln C_v versus ln T plot and

Table 3 Bond lengths in the structure of $Bi_4Ti_3O_{12}$

Bond	*d*/Å	Bond	*d*/Å
$T = 173$ K			
Bi_1–O_5 (×4)	2.656 (11)	Ti_1–O_1 (×4)	1.9170 (1)
Bi_1–O_3 (×2)	2.7035 (12)	Ti_1–O_3 (×2)	2.305 (30)
Bi_1–O_3 (×2)	2.7230 (12)	Ti_2–O_4 (×1)	1.782 (27)
Bi_1–O_1 (×4)	2.915 (1)	Ti_2–O_5 (×4)	1.932 (3)
Bi_2–O_2 (×4)	2.303 (1)	Ti_2–O_3 (×1)	1.967 (29)
Bi_2–O_4 (×2)	2.837 (8)		
Bi_2–O_4 (×2)	2.856 (8)		
$T = 273$ K			
Bi_1–O_5 (× 4)	2.635 (11)	Ti_1–O_1 (×4)	1.9168 (1)
Bi_1–O_3 (×2)	2.7019 (5)	Ti_1–O_3 (×2)	2.142 (25)
Bi_1–O_3 (×2)	2.7209 (5)	Ti_2–O_4 (×1)	1.668 (26)
Bi_1–O_1 (×4)	2.916 (1)	Ti_2–O_5 (×4)	1.934 (3)
Bi_2–O_2 (×4)	2.307 (1)	Ti_2–O_3 (×1)	2.119 (25)
Bi_2–O_4 (×2)	2.875 (9)		
Bi_2–O_4 (×2)	2.893 (9)		
$T = 373$ K			
Bi_1–O_5 (×4)	2.572 (11)	Ti_1–O_1 (×4)	1.9196 (1)
Bi_1–O_3 (×2)	2.7062 (5)	Ti_1–O_3 (×2)	2.142 (23)
Bi_1–O_3 (×2)	2.7246 (5)	Ti_2–O_4 (×1)	1.679 (25)
Bi_1–O_1 (×4)	2.922 (1)	Ti_2–O_5 (×4)	1.948 (3)
Bi_2–O_2 (×4)	2.308 (1)	Ti_2–O_3 (×1)	2.103 (23)
Bi_2–O_4 (×2)	2.887 (9)		
Bi_2–O_4 (×2)	2.904 (9)		
$T = 473$ K			
Bi_1–O_5 (×4)	2.570 (11)	Ti_1–O_1 (×4)	1.9212 (1)
Bi_1–O_3 (×2)	2.7087 (5)	Ti_1–O_3 (×2)	2.261 (26)
Bi_1–O_3 (×2)	2.7264 (5)	Ti_2–O_4 (×1)	1.817 (25)
Bi_1–O_1 (×4)	2.925 (1)	Ti_2–O_5 (×4)	1.954 (4)
Bi_2–O_2 (×4)	2.310 (1)	Ti_2–O_3 (×1)	2.005 (25)
Bi_2–O_4 (×2)	2.840 (8)		
Bi_2–O_4 (×2)	2.857 (8)		

Eq. (4), it was found that in the range 25–50 K, $D = 1.6$, $\theta_{max} = 237.0$ K for tetrabismuth trititanium oxide. With these values of D and θ_{max}, Eq. (4) reproduces the experimental C_p^o values in the temperature range mentioned with an uncertainty of ±0.36 %. The D-value points to the chain-layered structure of $Bi_4Ti_3O_{12}$ [14–17].

Standard thermodynamic functions

To calculate the standard thermodynamic functions (Table 5) of the tetrabismuth trititanium oxide, its C_p^o values were extrapolated from the temperature of the measurement beginning at approximately 7 to 0 K by graphic method [18]. The calculations of $H^o(T) - H^o(0)$ and $S^o(T) - S^o(0)$ were made by the numerical integration of $C_p^o = f(T)$ and $C_p^o = f(\ln T)$ curves, respectively, and the Gibbs function $G^o(T) - H^o(0)$ was estimated from the enthalpies and entropies at the corresponding temperatures [19]. It was suggested that the error of the function values was ±1 % at $T < 40$ K, ±0.5 % between 40 and 80 K and ±0.2 % in the range from 80 to 346 K.

The absolute entropies of tetrabismuth trititanium oxide (Table 5) and the corresponding simple substances Bi (cr), Ti (cr), and O_2 (g) [20, 21] were used to calculate the standard entropy of formation of the compound under study at 298.15 K, $\Delta_f S^o(298.15, Bi_4Ti_3O_{12}, cr) = -1086.6 \pm 0.8$ J K^{-1} mol^{-1}.

Differential scanning calorimetry and thermal deformation model

Joint application of X-ray diffraction studies depending on the temperature and differential thermal analysis made it possible to establish some peculiarities of processes taking place in the compound under investigation during heating. Figure 3 represents DTA curve of $Bi_4Ti_3O_{12}$, where we can see reversible endothermic effect at 934 K. This effect corresponds to reversible second-order transitions associated with sharp changes in the symmetry of the material, which can be characterized by a Curie temperature (T_C) ("normal" ferroelectric behavior) according to our research [4] and works [22, 23]. Melting compound corresponds to a second large endothermic effect at 1476 K.

Table 4 Coefficients in the fitting polynomials for $Bi_4Ti_3O_{12}$

T (K) Polynomial type	10–30 1	21–346 2
A/H	−3077.55301/−578940.180	3.79077379/−8.17451683
B/I	46061.6914/1403198.10	1.46366760/17.1864846
C/J	−294418.904/−825311.032	−0.558354072/−16.8129445
D/K	1042994.11/174507.130	0.059611395/9.31312689
E/L	−2200119.15	0.441530165/−3.00663053
F/M	2686842.37	0.804927908/0.529217814
G/N	−1451692.55	−0.022092694/−0.039360306

Table 5 Thermodynamic functions of crystalline $Bi_4Ti_3O_{12}$; $M = 1171.515$ g mol^{-1}, $p^o = 0.1$ MPa

T (K)	$C_p^o(T)$/J K^{-1} mol^{-1}	$H^o(T) - H^o(0)$/kJ mol^{-1}	$S^o(T)$/J K^{-1} mol^{-1}	$-[G^o(T) - H^o(0)]$/kJ mol^{-1}
0	0	0	0	0
5	1.832	0.0032	0.9619	0.00157
10	6.372	0.0228	3.488	0.01208
15	13.27	0.0709	7.297	0.0386
20	22.43	0.1587	12.28	0.0870
25	33.29	0.2979	18.45	0.1634
30	44.29	0.4920	25.50	0.2730
35	54.80	0.7400	33.13	0.4194
40	64.78	0.1039	41.10	0.6049
45	74.51	1.387	49.29	0.8308
50	84.23	1.784	57.64	1.098
60	103.8	2.724	74.73	1.760
70	123.2	3.860	92.20	2.594
80	142.0	5.186	109.9	3.604
90	160.2	6.697	127.7	4.792
100	178.0	8.389	145.5	6.158
110	195.5	10.26	163.2	7.701
120	212.4	12.30	181.0	9.422
130	228.6	14.50	198.6	11.32
140	244.0	16.87	216.1	13.39
150	258.5	19.38	233.5	15.64
160	272.1	22.03	250.6	18.06
170	285.0	24.82	267.5	20.65
180	297.3	27.73	284.1	23.41
190	309.2	30.76	300.5	26.34
200	320.7	33.91	316.7	29.42
210	332.0	37.18	332.6	32.67
220	343.1	40.55	348.3	36.07
230	353.9	44.04	363.8	39.63
240	364.5	47.63	379.1	43.35
250	374.8	51.33	394.2	47.21
260	384.6	55.12	409.1	51.23
270	394.2	59.02	423.8	55.39
273.15	397.1	60.26	428.3	56.74
280	403.4	63.01	438.3	59.71
290	412.3	67.08	452.6	64.16
298.15	419.4	70.47	464.1	67.89
300	421.0	71.25	466.7	68.76
310	429.6	75.50	480.6	73.49
320	438.2	79.84	494.4	78.37
330	446.7	84.27	508.0	83.38
340	455.2	88.78	521.5	88.53
346	460.2	91.52	529.5	91.68

$u(C_p^o(T)) = \pm 2$ % ($5 < T < 20$ K); ± 0.5 % ($20 < T < 40$ K); ± 0.2 % ($T > 40$ K) (level of confidence = 0.95), $u(p) = \pm 1$ %

In the next stage of our work, we decided to clarify the mechanisms of atomic displacements in the ferroelectric phase, which lead later to a second-order transition (T_C). Our research has shown that most "mobile" atoms are O_3, O_4, O_5 in slabs and Bi_2 in blocks. The displacements of these atoms are shown by the arrows in Fig. 2b, c. The

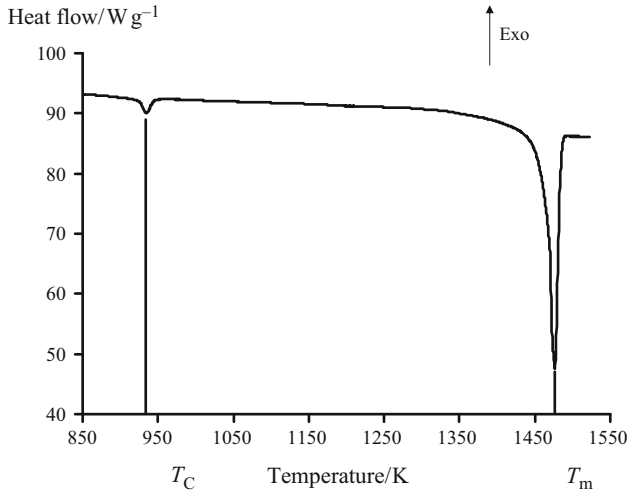

Fig. 3 DTA curve of $Bi_4Ti_3O_{12}$

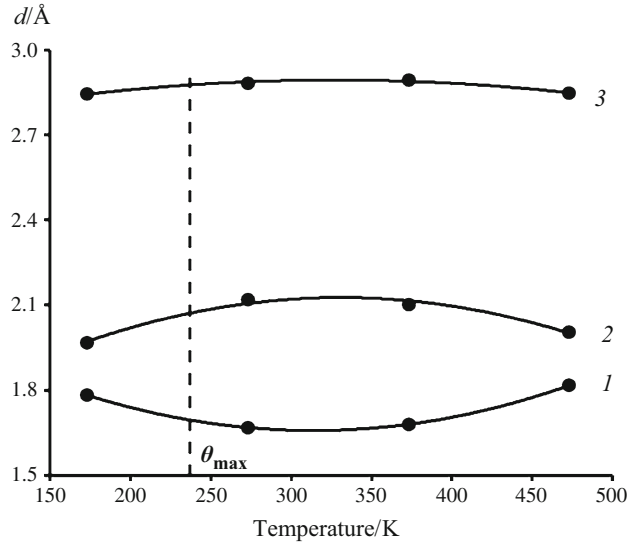

Fig. 4 Temperature dependence of bond lengths in crystal structure of $Bi_4Ti_3O_{12}$ (*1*—Ti_2–O_4; *2*—Ti_2–O_3; *2*—average Bi_2–O_4)

most significant displacement of the atoms is observed for the oxygen atoms in the outer octahedra of slabs (Fig. 2b). Bismuth atoms in the blocks move much less (Fig. 2c). All movements occur along the crystallographic *c* axis. We have noted that the direction of movement essentially depends on temperature. The distortion of octahedra in the slabs is observed at temperatures down to θ_{max} (Fig. 4). On the contrary, at higher temperatures occurs gradually alignment of the bond lengths in the octahedra. This process leads to an increase in the symmetry of the structure and phase transition. Thus, the symmetrization of the octahedra in the slab is the main reason of transition for ferroelectric Aurivillius phases in the paraelectric phase.

Conclusions

The temperature dependence of heat capacity of $Bi_4Ti_3O_{12}$ has been measured in the range from 7 to 346 K by precision adiabatic vacuum calorimetry. The experimental data were used to calculate standard thermodynamic functions. We have studied the mechanism of thermal deformations in the Aurivillius phase.

Acknowledgements The work was performed with the financial support of the Russian Foundation of Basic Research (Project Number 13-03-00152).

References

1. Aurivillius B. The structure of Bi_2NbO_5F and isomorphous compounds. Arkiv foer Kemi. 1952;4:39–47.
2. Aurivillius B. Mixed bismuth oxides with layer lattices. I. The structure type of $CaNb_2Bi_2O_9$. Arkiv foer. Kemi. 1949;1:463–80.
3. Aleksandrov KS, Beznosikov BV. Perovskity. Nastoyashchee i budushchee. (Mnogoobrazie prafaz, fazovye prevrashcheniya, vozmozhnosti sinteza novykh soedinenii) (Perovskites: Critical Issues and Future Prospects (Diversity of Parent Phases, Phase Transformations, and the Possibility of the Synthesis of New Compounds)), Novosibirsk: Sib. Otd. Ross. Akad. Nauk, 2004, p. 231.
4. Knyazev AV, Krasheninnikova OV, Korokin VZh. High-temperature characterization of some Aurivillius phases. Inorg Mater. 2014;50(2):170–8.
5. Wang CM, Wang JF, Gai ZG. Enhancement of dielectric and piezoelectric properties of $M_{0.5}Bi_{4.5}Ti_4O_{15}$ (M = Na, K, Li) ceramics by Ce doping. Scripta Mater. 2007;57(9):789–92.
6. Araujo CAP, Cuchiaro JD, McMillan LD, Scott MC, Scott JF. Fatigue-free ferroelectric capacitors with platinum electrodes. Nature. 1995;374(6523):627–9.
7. Subbarao EC. A family of ferroelectric bismuth compounds. J Phys Chem Solids. 1962;23(6):665–76.
8. Rietveld HM. Line profiles of neutron powder-diffraction peaks for structure refinement. Acta Crystallogr. 1967;22(Part 1):151–2.
9. Izumi F, Young RA. The rietveld method, Oxford University Press, Oxford, chap. 13, 1993.
10. Lebedev BV. Application of precise calorimetry in study of polymers and polymerization processes. Thermochim Acta. 1997;297:143–9.
11. Aurivillius B. Mixed bismuth oxides with layer lattices. II. Structure of $Bi_4Ti_3O_{12}$. Arkiv foer Kemi. 1949;1:499–512.
12. Yakubov TS. On the specific heat of solids that exhibit fractal character. Dokl Acad Sci. 1990;310:145–50.
13. Tarasov VV. The theory of the heat capacity of chain-layered structures. Zhurnal Fiz Khimii. 1950;24:111–28.
14. Knyazev AV, Smirnova NN, Mączka M, Knyazeva SS, Letyanina IA. Thermodynamic and spectroscopic properties of spinel with the formula $Li_{4/3}Ti_{5/3}O_4$. Thermochim Acta. 2013;559:40–5.
15. Chernorukov NG, Smirnova NN, Knyazev AV, Marochkina MN, Bykova TA, Ershova AV. The thermodynamic properties of calcium uranoborate. Russ J Phys Chem. 2006;80(1):37–41.
16. Karyakin NV, Chernorukov NG, Suleimanov EV, Alimzhanov MI, Trostin VL, Knyazev AV. The thermodynamic properties of uranyl pyrovanadate and uranovanadic acid. Russ J Phys Chem. 2000;74:1226–31.

17. Knyazev AV, Mączka M, Kuznetsova NYu, Hanuza J, Markin AV. Thermodynamic properties of rubidium niobium tungsten oxide. J Therm Anal Calorim. 2009;98:843–8.
18. Knyazev AV, Smirnova NN, Mączka M, Hermanowicz K, Knyazeva SS, Letyanina IA, Lelet MI. Thermodynamic and spectroscopic properties of $Co_{7/3}Sb_{2/3}O_4$. J Chem Thermodyn. 2014;74:201–8.
19. Lebedev BV. Application of precise calorimetry in study of polymers and polymerization processes. Thermochim Acta. 1997;297:143–9.
20. Cox JD, Wagman DD, Medvedev VA. Codata key values for thermodynamics, New York: Hemisphere Publishing Corp., 1984.
21. Chase MW Jr. NIST-JANAF themochemical tables, fourth edition. J Phys Chem Ref Data, Monograph. 1998;9:1–1951.
22. Lazarevic Z, Stojanovic BD, Varela JA. An approach to analyzing synthesis, structure and properties of bismuth titanate ceramics. Sci Sinter. 2005;37:199–216.
23. Naz S, Durrani SK, Qureshi AH, Hussain MA, Hussain N. Nanosized bismuth titanate ($Bi_4Ti_3O_{12}$) system drive through auto-combustion process by using suspension titania (TiO_2). J Therm Anal Calorim. 2014;115:587–93.